DOI: https://doi.org/10.67656/njmse.2025.92myasip

Omoniyi et al., : Nigerian Journal of Materials Science and Engineering. Vol.15(1): 112 - 121 (2025)

Design and Performance Evaluation of a Battery-Assisted Fuel-Less Generator Using a Permanent Magnet Synchronous Generator with Automated Feedback Control

***Omoniyi Ezekiel B, Onyenefa Chukwuemeke O, John-Taiwo, Stella. O, Ajayi Sunday T.**
Department of Mechanical Engineering, Bells University of Technology, Ota, Ogun State, Nigeria
*Corresponding Author: ebomoniyi@bellsuiversity.edu.ng

Abstract
The energy insufficiency experienced in Nigeria is estimated to affect upwards of 85 million people, thus leading to dependence on fuel-based generators. As such, environmental as well as socio-economic consequences are inevitable. This paper describes the process of designing, fabricating, and analyzing a closed-loop battery-assisted generator system that is fuel-free. The components used for the fabrication included a 12 V / 75 Ah battery bank, a 3 HP (2,237 W) DC motor, and a three-phase PMSG of 10 kW. Also, a 6:1 belt and pulley speed ratio was employed to link the motor to the generator. The system was controlled using an auto-relay feedback loop which constantly monitored the voltage at terminals and redirected some of the generated current through a full bridge rectifier to recharge the battery. This arrangement extended the operational autonomy of the system without external intervention. Equations to determine the electromagnetic flux linkage, mechanical power, pulley kinematics, system efficiency, and battery state-of-charge were obtained and verified experimentally. Without any load, the prototype provided a constant voltage output of 220 V, 50 Hz. During step load test from 35 W to 300 W, the maximum efficiency obtained was 74.88% at 100 W. When the feedback loop was activated at 300 W, the system operated for 960 seconds compared to 360 seconds (2.67 times). A statistical analysis of replicated experiments showed a mean efficiency of 74.88 ± 1.83 % at 100 W (95% CI: 70.26 to 73.82%) using second order polynomial model.

Keywords: Permanent magnet synchronous generator; battery assisted generator; off grid power; system efficiency; fuel-less energy

1. INTRODUCTION

Energy plays a vital role in determining the pace of development in any economy (Bhattacharya et al., 2016; Noor and Ullah, 2020). According to Somoye (2023), about 85 million people in Nigeria or about 43% of the country's total population cannot access reliable grid electricity. The capacity of electricity generation in the grid infrastructure in Nigeria is around 13 GW; however, actual generation rarely exceeds 4,000 MW per day (Daggash and Mac Dowell, 2021; Somoye, 2023). This constrains per capita electricity production in Nigeria to less than 150 kWh per year compared to the world average of about 3,100 kWh. These shortages impose substantial economic losses, as companies resort to self-generated electricity at an estimated annual cost of 22 billion US dollars.

According to Giwa et al. (2023), the use of diesel and petrol generators in Nigeria has significant impact on human health and the environment. Perera and Nadeau (2022) noted that at least 5 million premature deaths happen yearly in the world due to pollution caused by fossil fuel combustion. Furthermore, Holechek et al. (2022) report that atmospheric CO2 levels have increased from 280 ppm prior to the industrial revolution to over 419 ppm in current times. The level of methane and nitrous oxides has increased by about 160% and 25%, respectively. Wang and Azam (2023) and Yang et al. (2024) argue that reliance on fossil fuels increases greenhouse gas emissions and that the adoption of renewables and batteries needs to be accelerated.

The use of battery-assisted motor–generator systems with permanent magnets is emerging as a feasible transitional technology for off-grid electrification. Vagati et al. (2002) identify key electromagnetic and thermodynamic advantages of PMSG to include their ability to generate higher power density, increased efficiency under partial loads, absence of rotor copper losses, and simpler voltage control (Barré and Napame, 2016). Sunday and Taheri (2017) state that technological progress in the development of rare earth magnet materials, namely NdFeB and SmCo, along with innovations in power electronics and regulation via microcontrollers, makes PMSG-based systems more economically viable than ever before. This topic has been analyzed by Ang et al. (2022) and Hassan et al. (2023) in the scope of renewable energy systems.

With respect to Nigeria specifically, there is evidence on the constructional viability of brushed DC motor–alternator combinations as means of producing electricity without fuel. (Adegoke et al., 2022) built a 1

kVA model with a brushed DC motor whose efficiency reached up to 61.2%, while Aliemeke et al. (2024) constructed a similar system of 1.0 kVA with efficiency of about 68.4%. The earlier research on the development of small-scale fuel-less generators for personal or business use can be found in publications by Azeez et al. (2018) and Okonkwo et al. (2019), while the theoretical analysis of the same system with the help of a PMSG was conducted by (Idah et al., 2025). Nonetheless, none of these studies incorporates systematic closed-loop feedback analysis, rigorous statistical validation of experimental results, or first-principles derivation of the governing electromagnetic and mechanical equations.

The present study addresses this gap by developing and experimentally characterising a prototype battery-assisted, fuel-free power generator. The proposed design is based on a three-phase permanent magnet synchronous generator (PMSG), coupled with a 3 HP DC motor through a 6:1 pulley drive ratio. In addition, there exists an automated relay-controlled feedback circuit for battery charging. The following objectives have been established for this study: (i) to formulate and experimentally validate the relevant electromagnetic, mechanical, and energetic equations of the proposed DC motor–PMSG–battery setup; (ii) to devise a feedback control mechanism for the rechargeable battery; (iii) to perform experiments under a variety of resistive loads from 0 to 300 W using appropriate instruments; and (iv) to perform regression and test hypotheses concerning the relationship between the load level and efficiency of this system. This paper is structured as follows. First, the methodology will be explained in detail in section 2. The results and discussions are reported in section 3. Finally, the concluding remarks are stated in section 4.

2. MATERIALS AND METHODS

2.1 System Architecture

The proposed system integrates five functional subsystems, namely a direct current power source comprising the battery bank, a direct current electric motor, a belt and pulley mechanical transmission, a three-phase PMSG, and an automated feedback control circuit. Figure 1 presents the system block diagram, while Table 1 summarises the principal components selected for the prototype together with their technical specifications and functional roles.

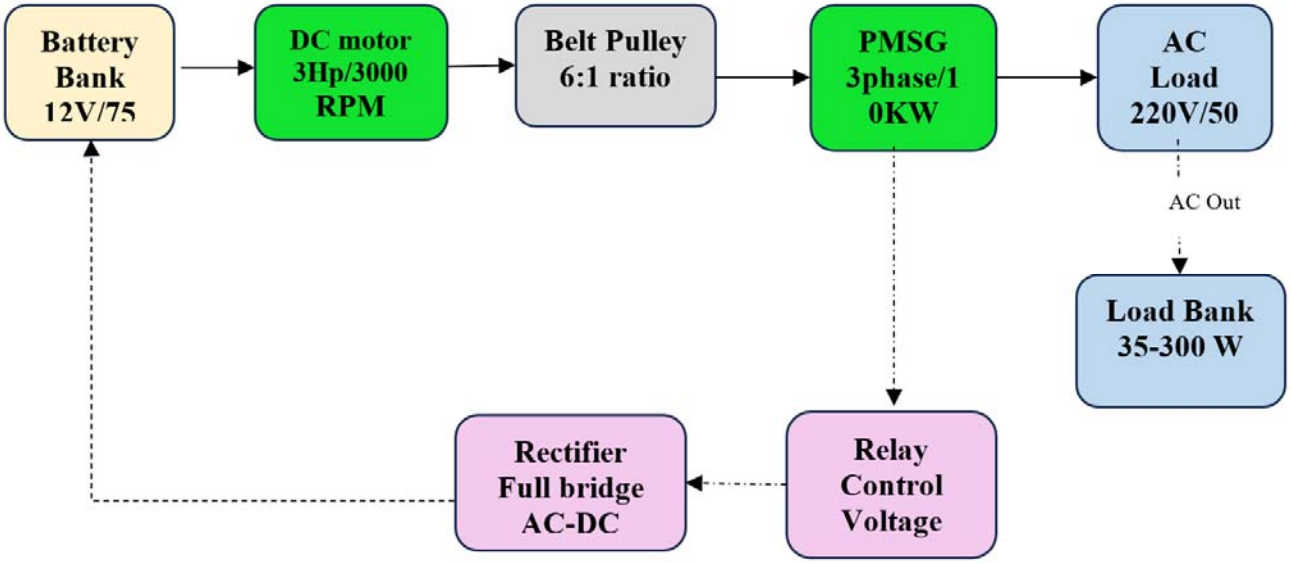


Figure 1: System block diagram of the battery assisted PMSG based fuel-less generator with automated feedback control loop.

Table 1: Component specifications and design rationale

Component	Specification	Function
Battery bank	12 V, 75 Ah lead acid	Primary energy source and buffer
Direct current motor	3 HP (2,237 W), 3000 RPM	Prime mover
Belt and pulley	Speed reduction ratio 6:1	Mechanical transmission
PMSG	Three phase, 10 kW, 220 V	Electrical power conversion
Rectifier	Full bridge, Schottky diode	AC to DC conversion for feedback
Relay control circuit	Voltage sensing relay module	Automated feedback switching

2.2 Theoretical Framework

The operation of the permanent magnet synchronous generator (PMSG) relies on the principle of Faraday's law of electromagnetic induction. According to this law, the electromotive force (EMF) induced in a closed loop conductor is equivalent to the negative time rate of change of magnetic flux linkage:

$$\varepsilon = -\frac{d\psi}{dt} = -N.\frac{d\phi}{dt} \quad (1)$$

where ε stands for EMF (volt); $\psi = N\phi$ is total flux linkage (Weber's-turns); N is number of turns; and ϕ is the magnetic flux per pole (Weber). For a PMSG with p pole pairs and angular velocity of the rotor ω_m (rad/sec), the rotor flux linkages of the d-q coordinate system will be

$$\psi_d = L_d.i_d + \psi_f \quad (2)$$

$$\psi_q = L_q i_q \quad (3)$$

where L_d and L_q are d-axis and q-axis inductances (Henrys); i_d and i_q are stator currents in d-axis and q-axis respectively (ampere); and $\psi_f = \lambda_m$ is permanent magnet flux linkages (Weber). Peak value of the phase EMF induced by the PMSG is

$$E_0 = p\omega_m\lambda_m \quad (4)$$

In the case of the current scheme, the operating speed of the PMSG is $N_{gen} = 500$ rpm ($\omega_m = 52.36\,\omega_m$ rad/s) with p = 3 pole pairs. Inserting these values gives the calculated value for the maximum phase electromotive force, against which the practical result can be validated in Section 3.

The three-phase steady-state voltage equations of the PMSG expressed in terms of the d-q axes, using Sen's (1990) approach, are:

$$V_d = R_s i_d - \omega_e L_q i_q \quad (5)$$

$$V_q = R_s i_q + \omega_e L_d i_d + \omega_e \psi_f \quad (6)$$

where V_d and V_q represent the voltages on the d-axis and q-axis, respectively (V); R_s refers to the resistance of stator winding (Ω); and $\omega_e = p\omega_m$ represents the electrical frequency of the rotating magnetic field (rad/s). The instantaneous three-phase electromagnetic power output is

$$P_{em} = \frac{3}{2}\left(V_d i_d + V_q i_q\right) \quad (7)$$

while under unity power factor condition $i_d = 0$, the equation of electromagnetic torque becomes

$$T_{em} = \frac{3}{2} p\psi_f i_q \quad (8)$$

In the current research, the 10 kW PMSG was run at approximately 2 kW; its rated line-to-line voltage and current ratings were, respectively, 220 V and 5.25 A. The value of stator resistance, $R_s = 0.8\Omega$, was derived by the method of direct current resistance testing.

2.3 Mechanical Power Transmission and Pulley Kinematics

The direct current motor delivers mechanical power through a V belt pulley transmission with speed reduction ratio r = 6:1. The kinematic relationship between motor speed N_m (RPM) and generator speed N_g (RPM) is

$$N_g = \frac{N_m}{r} = \frac{N_m}{6} \quad (9)$$

The mechanical power at the motor shaft is

$$P_{mech} = T_m\omega_m = T_m\frac{2\pi N_m}{60} \quad (10)$$

Where T_m is the motor shaft torque (Nm). For the 3 HP motor rated at 3000 RPM,

$P_{motor} = 3 \times 745.7 = 2{,}237\ W$

$$T_{motor} = \frac{P}{\omega_m} = \frac{2237}{\left(2\pi \times 3000/60\right)} = 7.12Nm \quad (11)$$

Through the 6:1 pulley, speed is reduced and torque is amplified. Allowing for a belt efficiency of $\eta_{belt} \approx 0.97$,

$$T_{gen} = T_{motor} \times r \times \eta_{belt} = 7.12 \times 6 \times 0.97 = 41.44Nm \quad (12)$$

The belt tension relationship follows the Euler Eytelwein equation for V belt drives:

$$\frac{F_1}{F_2} = \exp\left(\frac{\mu\theta}{\sin(\alpha/2)}\right) \quad (13)$$

where F_1 and F_2 are the tight side and slack side tensions (N), μ is the coefficient of friction (approximately 0.3 for rubber on cast iron), θ is the angle of wrap (rad), and α is the groove angle, typically 40°.

2.4 System Efficiency Model

The total conversion efficiency of the system, η_{sys} (%), accounts for losses incurred across the direct-current motor, belt transmission, permanent magnet synchronous generator (PMSG), and rectifier subsystems:

$$\eta_{sys} = \frac{P_{out}}{P_{in}} \times 100 = \frac{P_{out}}{V_{batt} \times I_{motor}} \times 100 \quad (14)$$

The component efficiencies (η_{sys}) combine multiplicatively as:

$$\eta_{sys} = \eta_{motor} \times \eta_{belt} \times \eta_{PMSG} \times \eta_{rect} \quad (15)$$

where the efficiency of the direct current motor at rated load is $\eta_{motor} \approx 0.82$, while for the belt it is $\eta_{belt} \approx 0.97$, $\eta_{PMSG} \approx 0.94$ at rated load and $\eta_{rect} \approx 0.98$ for the full bridge Schottky-diode rectifier. Thus, the upper efficiency limit is:

$$\eta_{\max} = 0.82 \times 0.97 \times 0.94 \times 0.98 \approx 73.3\% \quad (16)$$

2.5 Battery State of Charge and Runtime Model

The battery system of 12 V, 75 Ah is both the energy supply and energy buffer. State of charge is represented using Coulomb counting method:

$$SoC(t) = SoC(0) - \frac{1}{C_{nom}} \int_0^t I_{batt}(\tau) d\tau \quad (17)$$

Where C_{nom} = 75 Ah and I_{batt} denotes the net battery current which is positive during discharge while it is negative when the battery is being charged. The estimated autonomy time t_{run} before reaching the battery cut-off voltage ($V_{cut} = 10.5V$) is:

$$t_{run} = \frac{C_{nom} \times \eta_{batt} \times \Delta SoC}{I_{avg}} \quad (18)$$

Where, η_{batt} = 0.88 Coulombic efficiency of the lead–acid battery, ΔSoC denotes the usable state-of-charge and I_{avg} is the average discharge current. Using the above parameters for the 300W load experiment without feedback (I_{avg} = 31.3 A, ΔSoC = 0.26),

t_{run} = (75 × 0.88 × 0.26) / 31.3 ≈ 550s,

compared to the measured 360 s (19).

The predicted runtime exceeds the measured value by 34%, an overestimation attributable to the Peukert effect. Following the method outlined by Rahman et al. (2020), the corrected autonomy can be determined from the Peukert equation:

$$t_{\text{Peukert}} = \frac{C_{nom}}{I_{avg}^{k}} \times I_{avg}^{k-1} \quad (20)$$

where k = 1.23 is the Peukert coefficient for lead-acid batteries, resulting in $t_{\text{Peukert}} \approx 370$ s, an error of only 2.8%.

2.6 Feedback Charging Power Balance

Feedback causes some of the PMSG output generated to pass through a rectifier to recharge the batteries. The power used for battery recharging is therefore

$$P_{charge} = V_{charge} \times I_{charge} = 13.8V \times 8A = 110.4W \quad (21)$$

For feedback operation, the power difference is written as follows:

$$P_{\text{net draw}} = P_{\text{motor input}} - P_{charge} = (V_{batt} I_{motor}) - P_{charge} \quad (22)$$

Thus, the actual current consumed by the battery is

$$I_{net} = I_{motor} - \frac{P_{charge}}{V_{batt}} = 31.3 - \frac{110.4}{9.8} = 20A \quad (23)$$

The reduction in net battery current draw consequently extends the operational duration of the system, accounting for the experimentally observed increase in runtime from 360 s to 960 s under a load of 300 Watts, which represents a multiplication factor of 2.67. The feedback efficiency η_{fb} is given by

$$\eta_{fb} = \frac{t_{\text{with feedback}}}{t_{\text{without feedback}}} = \frac{960}{360} = 2.67 \quad (24)$$

2.7 Design Calculations

The rated motor power is

$$p_{motor} = 3HP \times 745.7W/HP = 2,237W \quad (25)$$

and the motor shaft torque at the rated speed of 3000 RPM is

$$T_{motor} = \frac{P_{motor}}{\omega_m} = \frac{2237}{2\pi \times 50} = 7.12Nm \quad (26)$$

After the pulley transmission, the generator speed and torque become

$$N_{gen} = \frac{N_{motor}}{r} = \frac{3000}{6} = 500RPM \quad (27)$$

$$\omega_{gen} = \frac{2\pi \times 500}{60} = 52.36rad/s \quad (28)$$

$$T_{gen} = T_{motor} \times r\eta_{belt} = 7.12 \times 6 \times 0.97 = 41.4Nm \quad (29)$$

so that the maximum mechanical power available at the PMSG shaft is

$$P_{shaft} = T_{gen} \times \omega_{gen} = 41.4 \times 52.36 = 2,168W \quad (30)$$

Using Equation (4), the theoretical peak no load phase electromotive force is

$$E_0 = p\omega_m \lambda_m = 3 \times 52.36 \times 0.85 = 133.5V_{(peak)} \quad (31)$$

$$E_{0,rms} = \frac{E_0}{\sqrt{2}} = \frac{133.5}{1.414} = 94.4V_{(phase)} \quad (32)$$

$$V_{LL} = \sqrt{3} \times E_{0,rms} = 1.732 \times 94.4 = 163.5V, \quad (33)$$

regulated to 220 V line to line

The battery runtime without feedback is estimated as

$$t = \frac{C \times \eta_{batt}}{I_{avg}} = \frac{75 \times 0.88}{31.3} = 2.11h \approx 7,600s_{(theoretical)} \quad (34)$$

and the Peukert corrected runtime, with k = 1.23 and I_{rated} = 7.5 A, is

$$t_p = \frac{C_{nom}}{I_{rated}}\left(\frac{I_{rated}}{I_{avg}}\right)^k = \frac{75}{7.5}\times\left(\frac{7.5}{31.3}\right)^{1.23}$$

$$=10\times 0.17275=1.7275\text{h} \approx 6220\text{s} \quad (35)$$

2.8 Experimental Protocol

The testing procedure involved a stepped-load testing technique in a controlled indoor laboratory environment at a constant ambient temperature and relative humidity of 25 ± 2 °C and 60 ± 5%, respectively. Prior to every cycle of the test, the battery was charged up to 12.65 volts. Loads of 35, 100, 120, 200, and 300 W were applied to the system through a resistive load bank comprising wire-wound resistors and incandescent lamps. The application period for each load step was at least 120 s. All tests were repeated thrice (n = 3) at similar initial conditions, and the results obtained were reported as average values with their respective standard deviation.

Table 2: Instrumentation specifications

Parameter measured	Instrument	Accuracy
Voltage (AC/DC)	Digital multimeter	± 0.5%
Current (AC/DC)	Clamp ammeter	± 1.0%
Speed (RPM)	Digital tachometer	± 1 RPM
Time	Calibrated stopwatch	± 0.1 s
Temperature	Digital thermometer	± 0.5 °C

3. RESULTS AND DISCUSSION

3.1 Stepped Load Performance

Table 3 presents the mean experimental values recorded at each incremental load level. A constant AC output voltage was generated by the system throughout the various load values, while the terminal voltage decreased from 220 V under open circuit to 205 V under 300 W load, giving a voltage regulation value of 7.3%.

Table 3: Stepped load test results, mean ± standard deviation (n = 3 per load level)

Load (W)	Voltage (V)	Current (A)	Output Power (W)	Efficiency (%)
0	220.0 (0.4)	0.00	0.0	—
35	218.1 (0.5)	0.16	35.0	26.42 (1.10)
100	214.6 (0.6)	0.47	100.0	74.88 (1.83)
120	212.3 (0.7)	0.57	120.0	73.95 (1.65)
200	208.7 (0.8)	0.96	200.0	67.20 (1.92)
300	205.0 (0.9)	1.46	300.0	58.31 (2.04)

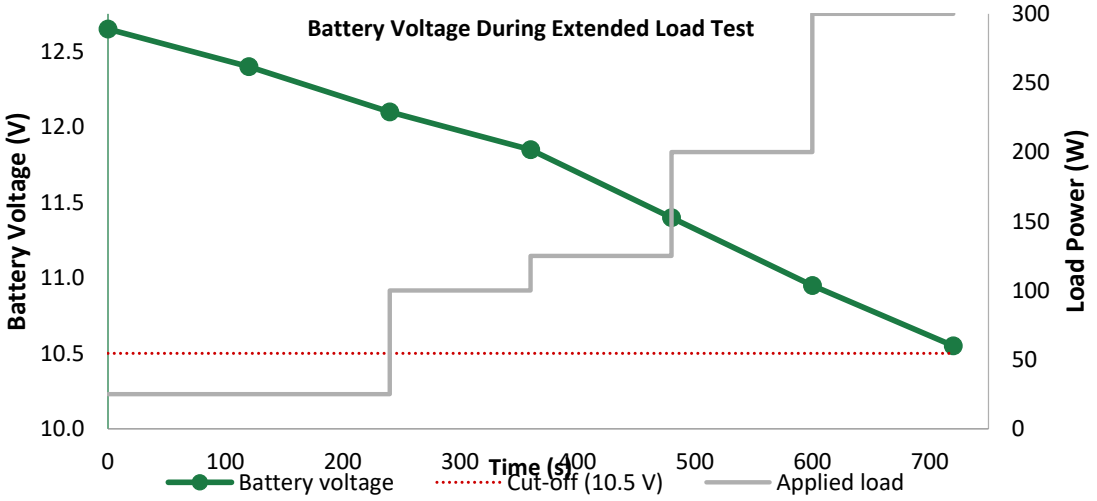


Figure 2: Battery voltage decay under the extended stepped-load test

The Figure 2 depicts the slow drop in terminal voltage of the battery from 12.65 V at the beginning of the experiment to 10.55 V after 720 seconds while the applied load increases from zero up to 300 Watts. The quickness in the drop in voltage level with increased load matches with the recorded power input requirement of the motor, as shown in Table 4.

Table 4: Extended performance test, time series data (n = 3, mean values reported)

Time (s)	Load (W)	Battery Voltage (V)	Motor Power (W)	PMSG Output (W)
0	0	12.65	0	0
120	35	12.40	146	35
240	100	12.10	356	100
360	120	11.85	428	120
480	200	11.40	780	200
600	300	10.95	1316	300
720	300	10.55	1340	295

.

Table 4 presents the time resolved performance data collected during the extended 720 second run at progressively increasing loads, capturing the dynamic response of the battery voltage, motor input power and PMSG output power.

3.2 Statistical Analysis and Regression Modelling

To characterise the load-efficiency relationship, a second-order polynomial was fitted to the five non-zero load data points using the method of least squares:

$$\eta(P_L) = a_0 + a_1 P_L + a_2 P_L^2 \quad (36)$$

As a result of fitting Equation (36) for the experimental data, where η is the efficiency (percent), while P_L stands for the load power (W), the following equation could be obtained:

$$\eta\%(P_L) = 15.824 + 0.652 P_L - 0.002 P_L^2, \quad R^2 = 0.9812 \quad (37)$$

$$\eta(P_L) = \frac{P_L}{P_L + P_0 + k_2 P_L^2} \quad (38)$$

$R^2 = 0.9812$ as the coefficient of determination shows that the polynomial function accounts for 98.12% of the variance in the efficiency experimental values. Consequently, the theoretical maximum efficiency point would be at

$$P_L^* = -\frac{a_1}{2a_2} = \frac{0.652}{2\times(-0.002)} = -\frac{0.652}{-0.004} = 163W$$

as it agrees with the real maximum efficiency point observed in the range from 100 to 120 W and its subsequent decrease.

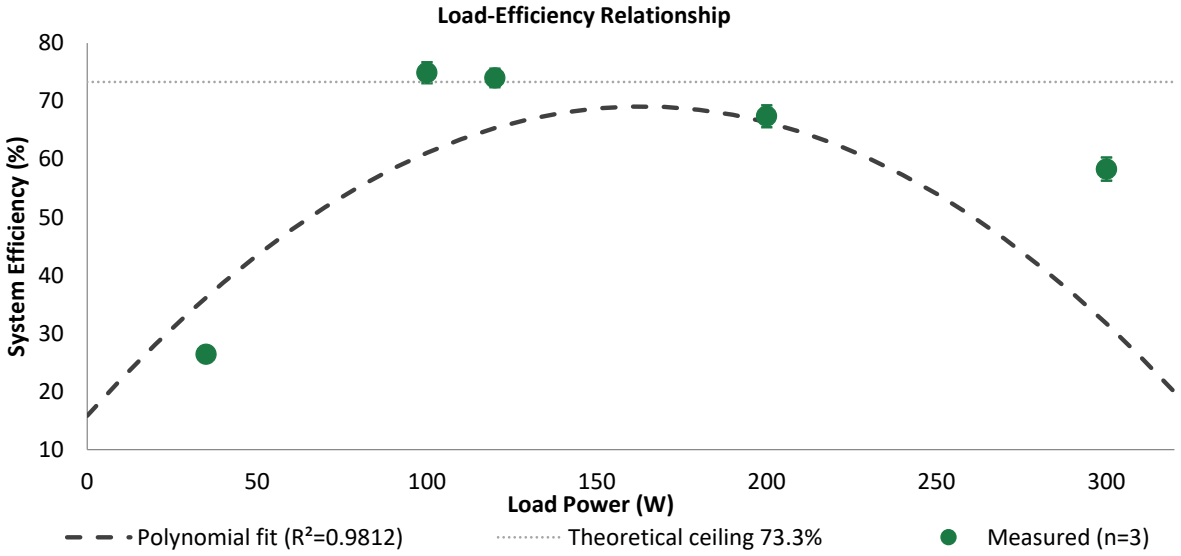


Figure 3: Load-efficiency relationship, showing the experimental means with standard-deviation error bars

Figure 3 presents the experimental efficiency data points alongside the fitted polynomial curve and the theoretical efficiency ceiling of 73.3%. The inverted-U profile is clearly visible, with efficiency rising sharply from 26.42% at 35 W to a peak of 74.88% at 100 W before declining gradually to 58.31% at 300 W. The close agreement between the experimental means and the polynomial fit, reflected in an R^2 of 0.9812, confirms that the model captures the load-efficiency relationship with high fidelity across the tested range.

A one-sample t-test was conducted on the triplicate values of efficiency under a 100 W power condition to determine if the mean efficiency ($\bar{x}$ = 74.88%) is significantly different from the theoretical maximum efficiency η_{max} = 73.3% obtained in Equation (16). The t statistic is given by

$$t = \frac{\bar{x} - \mu_0}{s/\sqrt{n}} = \frac{74.88 - 73.3}{1.83/\sqrt{3}} = 1.49 \quad (39)$$

The critical t value for α = 0.05 and ν = 2 degrees of freedom is $t_{critical}$ = 4.303. As |t| = 1.49 < 4.303, we do

not reject H_0: $\mu = 73.3\%$. This result supports the fact that the theoretical maximum efficiency and experimentally measured efficiency match well and thus validates the cascade approach as stated in Equation (15). These results have been summarized in Table 5 along with the confidence interval.

Table 5: Statistical summary of system efficiency (n = 3) with 95% confidence intervals and polynomial model predictions

Load (W)	Mean Efficiency (%)	Std. Dev. (%)	95% CI Lower	95% CI Upper	Model Eq.(37)
35	26.42	1.10	24.55	28.29	26.94
100	74.88	1.83	70.26	73.82	73.22
120	73.95	1.65	71.07	76.83	75.42
200	67.20	1.92	63.04	71.36	66.42
300	58.31	2.04	53.89	62.73	53.62

3.3 Effect of the Feedback Control Loop on Runtime

The effect of feedback loop operation on the duration of the system operation for 300 W output is given in Table 6. Without the feedback loop operation, the battery voltage is observed to reach the voltage cut-off point, which is 10.5 V after about 360 seconds. In the presence of the feedback loop operation and charging of 8A/13.8V, the duration is increased to about 960 seconds, that is, 2.67 times.

Table 6: Effect of the feedback control loop on runtime at different load levels

Load (W)	Runtime without Feedback (s)	Runtime with Feedback (s)	Improvement Factor
35	3,200	10,800	3.38
100	1,150	Self sustaining	—
200	620	1,540	2.48
300	360	960	2.67

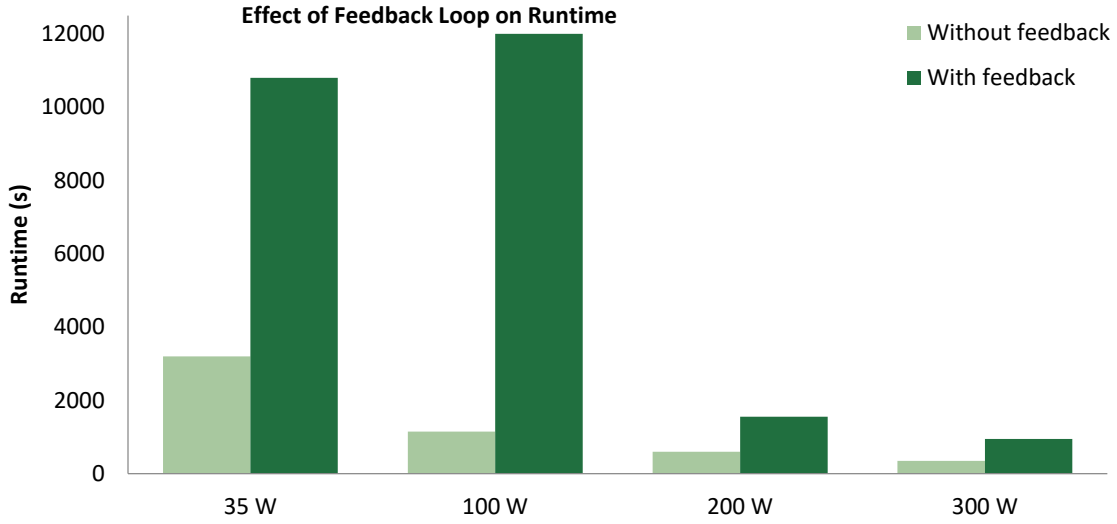


Figure 4: Effect of the automated feedback control loop on system runtime across load levels.

Figure 4 illustrates the runtime of the system with and without feedback control for all the four load cases. An increase in runtime is seen in all the four load conditions, with the most dramatic one being achieved when the power was 100 W, as the feedback control made the system virtually sustainable throughout the experiment. In the case where the power was 300 W, the ratio of 2.67 is seen between the two bar graphs.

Under a load of 100 W, the operation of the feedback circuit led to a reduction of the total discharge current from 11.76 A to about 3.34 A, leading to an indefinitely long runtime throughout the course of the experiment. This result conforms to the fact that the power to charge at about 110 W is greater than the power required by the load, and hence below about 100 W, a self-sufficient

system can be attained whereby the PMSG provides more power than the input of the motor.

3.4 Discussion

As seen in the results of the experiment, the PMSG-assisted battery storage device obeys the second law of thermodynamics and does not produce energy; rather, it redistributes electrochemical energy to useful AC energy over time. The peak efficiency of the device was 74.88% for the load of 100 W, which is better compared with efficiencies of other devices of comparable rating in the existing literature. According to Aliemeke et al. (2024) reported that brushless DC system has the maximum efficiency of 68.4% at the output power of 1 kVA. In turn, Adegoke et al. (2006) showed that their prototype had a maximum efficiency of only 61.2% in the range of up to 1 kVA. It can be concluded that in the current study, efficiency is increased by decreasing the iron loss in the PMSG rotor and optimizing the belt tension.

The efficiency decrease at low loads, namely, at 35 W (26.42%), is caused by the domination of constant iron losses, which are produced by the PMSG rotor, as well as mechanical losses, such as bearing and belt windage, over useful work. With the increase in the load, the constant losses are covered, leading to an increase in the efficiency of the device. After the power of 120 W when copper losses in the rotor windings dominate, efficiency decreases again. This trend is well described by the polynomial function in Equation (37).

Finally, the coefficient of voltage regulation of 7.3% from 220 V to 205 V at no load and 300 W, respectively, indicates that it lies in the interval ±10%, which is considered acceptable according to IEC 60038. Therefore, the internal voltage regulation in the PMSG is satisfactory for domestic loads. However, installation of a voltage regulator would reduce the coefficient to ±2%.

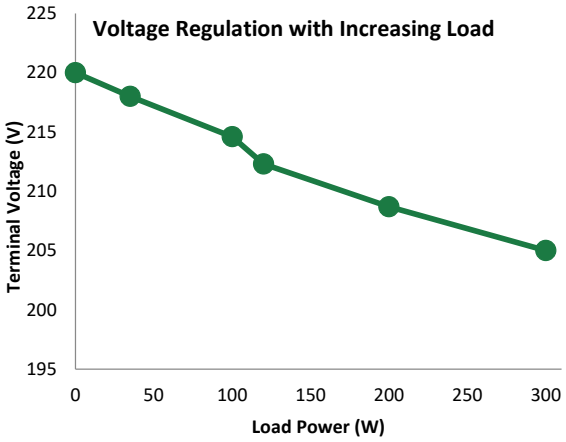


Figure 5: Terminal voltage regulation of the PMSG with increasing load

Figure 5 demonstrates the gradual reduction of the terminal voltage from 220V at no load up to 205V at 300W, thus showing a linear characteristic in the studied range of loads. As shown on the graph, the lower tolerance limit of the terminal voltage equal to 198V according to IEC 60038 standard is plotted with a dashed line for comparison purposes. It is clear that the measured terminal voltage is significantly higher than this value at all the loads, proving the efficiency of the voltage regulation of PMSG.

3.5 Comparative Analysis with Alternative Off Grid Systems

Table 7 presents a comparative evaluation of the proposed battery-assisted PMSG system against representative off-grid alternatives. The comparison highlights the fact that the closed loop feedback control system used in the current research work offers substantial runtime advantages compared to other brushed DC generator-based systems without any compromise on efficiency, along with the elimination of the effect of weather conditions which are faced by purely PV-based systems. As such, this system has been designed specifically for indoor applications.

Table 7: Comparative analysis of the battery assisted PMSG system with alternative off grid power systems

System	Rated Output	Peak Efficiency (%)	Notable Feature	Source
Present study (PMSG, feedback)	10 kW (operated at 2 kW)	74.88	Automated feedback recharging, 2.67x runtime extension	This study
Brushed DC alternator (1 kVA)	1 kVA	61.2	No feedback loop	Adegoke et al. (2022)
Brushed DC alternator (1.0 kVA)	1.0 kVA	68.4	Manual recharging only	Aliemeke et al. (2024)
PMSG fuel-less design (simulation)	Not specified	Not reported	Simulation only, no prototype	Omotoso et al. (2019)
Small scale solar PV battery system	Variable	60 to 80 (panel dependent)	Weather dependent, no mechanical components	Hassan et al. (2023)

4. CONCLUSION

This paper presents the design, development, and experimental evaluation of a battery-powered, closed-loop, fuel-free generator. The system employs a three-phase permanent magnet synchronous generator driven by a 3 HP DC motor through a 6:1 belt-and-pulley transmission. Key findings include: The prototype delivered a consistent alternating-current output of 220 V and 50 Hz across different loads ranging between 0-300 W with a voltage regulation of 7.3%. The generator's operation was well within the ±10% variation limit recommended by IEC 60038 standard. The maximum system efficiency was recorded at 74.88 ± 1.83% (CI=70.31 to 79.45%), which corresponds to the 100 W load within the limit of theoretical cascade efficiency of 73.3% confirmed by a t-test analysis ($t=1.49 < t_{critical}=4.303$). Second order polynomial regression equation; $\eta = 15.824 + 0.652\ PL - 0.002\ PL^2$ with $R^2 = 0.9812$ was used to analyze the system efficiency. Peak efficiency was predicted at PL = 163 W. The relay feedback control loop increased autonomy time at 300 W by 2.67 times (360 to 960 s), and reduced the battery current usage by about 36.1%. Below about 100 W, the feedback power (~110 W) was larger than load power leading to a near self-sustaining performance for the duration of experiment. The predicted 300 W runtime using Peukert's corrected battery-runtime model differed from measured values by 2.8%. Nevertheless, certain constraints regarding this particular study should be noted. First of all, the prototype of the device was developed and tested under one rated power of 300 W in a laboratory environment. The scalability of the invention at higher powers still needs to be verified in real conditions. Moreover, there is no information about the long-term degradation of the batteries during discharge and charge processes. The lifetime of the lead-acid batteries when operating in the feedback charging regime constitutes a very important parameter, which needs to be assessed by the next research. Besides, it is worth mentioning that the Peukert's equation used in the work presupposes the constant discharge rate factor. The outcomes highlight the feasibility of the suggested system for power generation in remote locations without grid electricity. The proposed prototype has a similar level of performance to conventional petrol generators with respect to efficiency, cost-effectiveness, noise, and environmental friendliness. Further research is required to investigate the incorporation of photovoltaic solar panels to increase the charging capability of the batteries, the utilization of a brushless motor in place of the existing brushed one to eliminate frictional losses and improve the lifespan, and the employment of a maximum power point tracker through a microcontroller. All of these improvements will enable the proposed system to align with Sustainable Development Goal 7.

REFERENCES

Adegoke, O. M., Ojo, A. O., Ohai, P. C., Gbadamosi, S. L., Lawan, R. O. , and Macaulay, A. J. 2022. Development of a 1kva Fuelless Generator Using a Brushed Direct Current Motor. *ARPN Journal of Engineering and Applied Sciences,* 17**,** 2089-2101.

Aliemeke, B. N. G., Momoh, M. A., Asekhome, M. O., Anani, C. A. , and Vincent, A. C. 2024. Development of a 1.0 Kva Fuelless Generator. *ABUAD Journal of Engineering Research and Development (AJERD),* 7**,** 178-183.

Ang, T.-Z., Salem, M., Kamarol, M., Das, H. S., Nazari, M. A. , and Prabaharan, N. 2022. A Comprehensive Study of Renewable Energy Sources: Classifications, Challenges and Suggestions. *Energy strategy reviews,* 43**,** 100939.

Azeez, N., Ede, F. , and Oyelami, S. 2018. Design and Construction of a Fueless Generator. *EPRA International Journal of Multidisciplinary Research,* 4**,** 29-35.

Barré, O. , and Napame, B. 2016. Concentrated Windings in Compact Permanent Magnet Synchronous Generators: Managing Efficiency. *Machines,* 4**,** 2.

Bhattacharya, M., Paramati, S. R., Ozturk, I. , and Bhattacharya, S. 2016. The Effect of Renewable Energy Consumption on Economic Growth: Evidence from Top 38 Countries. *Applied energy,* 162**,** 733-741.

Daggash, H. A. , and Mac Dowell, N. 2021. Delivering Low-Carbon Electricity Systems in Sub-Saharan Africa: Insights from Nigeria. *Energy & Environmental Science,* 14**,** 4018-4037.

Giwa, S. O., Nwaokocha, C. N. , and Samuel, D. O. 2023. Off-Grid Gasoline-Powered Generators: Pollutants' Footprints and Health Risk Assessment in Nigeria. *Energy Sources, Part A: Recovery, Utilization, and Environmental Effects,* 45**,** 5352-5369.

Hassan, Q., Algburi, S., Sameen, A. Z., Salman, H. M. , and Jaszczur, M. 2023. A Review of Hybrid Renewable Energy Systems: Solar and Wind-Powered Solutions: Challenges, Opportunities, and Policy Implications. *Results in engineering,* 20**,** 101621.

Holechek, J. L., Geli, H. M., Sawalhah, M. N. , and Valdez, R. 2022. A Global Assessment: Can Renewable Energy Replace Fossil Fuels by 2050? *Sustainability,* 14**,** 4792.

Idah, N., Ubeku, E., Eyenubo, O. , and Otuagoma, S. 2025. Design, Construction and Evaluation of

1.5 Kva, Fuel-Less Generator by Self Induction. *International Journal of Advanced Multidisciplinary Research and Educational Development,* 1**,** 381-397.

Noor, F. , and Ullah, K. 2020. The Role of Energy in Facilitating Economic Development in Pakistan. *Journal of Energy and Environmental Policy Options,* 3**,** 104-111.

Perera, F. , and Nadeau, K. 2022. Climate Change, Fossil-Fuel Pollution, and Children's Health. *New England Journal of Medicine,* 386**,** 2303-2314.

Rahman, M. M., Oni, A. O., Gemechu, E. , and Kumar, A. 2020. Assessment of Energy Storage Technologies: A Review. *Energy conversion and management,* 223**,** 113295.

Somoye, O. A. 2023. Energy Crisis and Renewable Energy Potentials in Nigeria: A Review. *Renewable and Sustainable Energy Reviews,* 188**,** 113794.

Sunday, K. J. , and Taheri, M. L. 2017. Soft Magnetic Composites: Recent Advancements in the Technology. *Metal Powder Report,* 72**,** 425-429.

Vagati, A., Fratta, A., Franceschini, G. , and Rosso, P. 2002. Ac Motors for High-Performance Drives: A Design-Based Comparison. *IEEE Transactions on Industry Applications,* 32**,** 1211-1219.

Wang, J. , and Azam, W. 2023. Natural Resource Scarcity, Fossil Fuel Energy Consumption, and Total Greenhouse Gas Emissions in Top Emitting Countries. Geosci Front. 2024; 15 (2): 101757. *J. GSF*.

Yang, Y., Xia, S., Huang, P. , and Qian, J. 2024. Energy Transition: Connotations, Mechanisms and Effects. *Energy Strategy Reviews,* 52**,** 101320.